

Topological phases of dipolar particles in elongated Wannier orbitals

Kai Sun,^{1,2} Erhai Zhao,^{3,4} and W. Vincent Liu^{4,5}

¹*Department of Physics, University of Illinois at Urbana-Champaign, 1110 West Green Street, Urbana, IL 61801*

²*Joint Quantum Institute and Condensed Matter Theory Center,*

Department of Physics, University of Maryland, College Park, MD 20742

³*Department of Physics and Astronomy, George Mason University, Fairfax, VA 22030*

⁴*Department of Physics and Astronomy, University of Pittsburgh, Pittsburgh, PA 15260*

⁵*Center for Cold Atom Physics, Chinese Academy of Sciences, Wuhan 430071, China*

(Dated: November 2, 2018)

We show that topological phases with fractional excitations can occur in two-dimensional ultracold dipolar gases on a particular class of optical lattices. Due to the dipolar interaction and lattice confinement, a quantum dimer model emerges naturally as the effective theory describing the low-energy behaviors of these systems under well-controlled approximations. The desired hierarchy of interaction energy scales is achieved by controlling the anisotropy of the orbital dimers and the dipole moments of particles. Experimental realization and detection of various phases are discussed, as well as the possible relevance for quantum computation.

PACS numbers: 67.85.-d 03.67.Lx 05.30.Pr 37.10.Jk

Unlike the ordered phase described by the Landau theory of phase transitions, a topological state is characterized by its response to the changing of topology of the underlying manifold, instead of a local order parameter associated with symmetry breaking [1]. Theoretically, these phases are described by topological field theories, in which the low-energy elementary excitations often carry fractional quantum numbers of the constituent particles, a phenomenon known as fractionalization. These fractional excitations offer a concrete setting from which new physics emerges, e.g., the realization of topological quantum computation ([2] and reference therein).

The most celebrated topological phases are perhaps the fractional quantum Hall (FQH) states described by the topological Chern-Simons gauge theory, whose low-energy excitations carry fractional charges and statistics of an electron. Another important example is the Z_2 topological phase in two-dimensional (2D) quantum dimer models (QDM) of frustrated spins, introduced by Rokhsar and Kivelson (RK) [3–5]. This novel phase is known as the resonating-valence-bond (RVB) state described by a topological Ising gauge theory and gives rise to deconfined fractional excitations such as spinons which carry spin 1/2 but zero charge [6–10].

In ultracold atomic/molecular systems, efforts have been made in realizing various topological phases. For example, states similar to the FQH states were proposed in rotating atomic gases [11]. There also have been suggestions to simulate QDM [12] and the RVB phase with ultracold atomic systems, but with the challenge of achieving the special nonlocal interaction as pointed out [12]. In fact, in contrast to its theoretical appeal, similar difficulties appear in most attempts to realize QDM and the RVB phase, for example, in the frustrated-Ising model [13, 14] and the easy-axis antiferromagnet [15, 16].

In this letter, we propose a different approach to realize and study the topological phases using ultracold

dipolar particles (atoms or molecules) in specifically designed, non-standard optical lattices, in part motivated by the recent experiments of polar molecules ([17–19] and references therein). We exploit two novel features: 1) the orbital degree of freedom controlled by optical lattice confinement, and 2) the long-range interaction associated with dipoles. Using a site-to-bond duality mapping [20], we show that the orbital motions on some optical lattices with dipolar interactions can be mapped onto a QDM: a particle in the elongated Wannier orbital on the optical lattice corresponds to a dimer on the dual lattice; and the dipolar interaction between particles enforces the “hard-core constraint” of the dimers. By tuning the optical lattice and the external field (the latter aligns the dipole moments), this system shows great tunability in exploring different phases of the QDM. For bosonic particles, within experimentally reasonable parameter ranges, we shall show that various phases can be stabilized, including conventional crystalline phases and a Z_2 topological phase. The latter is similar to the RVB phase of the QDM, and will be referred to as the orbital-RVB (ORVB). Experimental detection of these phases and the fractional excitations in the ORVB phase shall be discussed. More interestingly, the orbital dimers in our model system can be either bosonic or fermionic, depending on the statistics of the constituent particles, whereas the frustrated spin system only allows bosonic dimers. This opens a new possibility for studying fermionic QDM and even the mixture of dimers with different statistics.

Orbital dimers in 2D optical lattices. We focus on a concrete example, a 2D Kagome lattice constituted by anisotropic potential wells [Fig. 1(b)]. Due to this anisotropy, the Wannier wavefunction at each site would be elongated and would be considered as a “dimer” as shown below. Note that arbitrary lattice potential can be generated in 2D for example by projecting a holographic mask through an imaging system [21]. Such potential

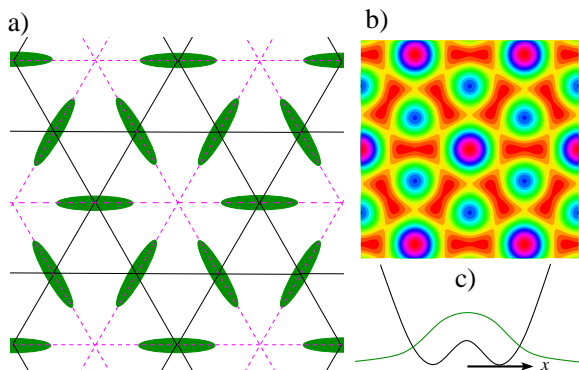


FIG. 1: (Color online) a) The Kagome lattice (solid lines) and its dual triangular lattice (dash lines). The green ellipse represents the elongated wavefunction at each site of the Kagome lattice (the bond of the triangular lattice). b) Contour plot of the 2D double-well optical lattice potential (with $I_2 = 2I_1$). Dipolar atoms (or molecules) reside at the intensity minima, which form the Kagome lattice. c) The local double-well potential and the wavefunction, which can be approximated by a Gaussian.

can also be achieved by independent sets of laser beams to produce an intensity pattern of (similar to Ref. [22])

$$I = I_1 \sum_{i=1,2,3} \cos^2(\mathbf{k}_i \cdot \mathbf{r}) + I_2 \sum_{j=1,2,3} \cos^2(\mathbf{q}_j \cdot \mathbf{r}), \quad (1)$$

where the amplitude of the wavevectors projected on the plane satisfy $|\mathbf{q}_j| = \sqrt{3}|\mathbf{k}_i|$ (the z component is irrelevant in a 2D system) and the azimuth angle of \mathbf{k}_i s (\mathbf{q}_j s) are $\theta_{\mathbf{k}_i} = i\pi/3$ ($\theta_{\mathbf{q}_j} = (j + 1/2)\pi/3$). This intensity pattern induces an optical lattice consisting of double-well-like potentials [Fig. 1(c)]. However, since the energy barrier between the two potential wells at one site is small, the double-well structure can be treated as a single anisotropic potential well, unless the energy of the trapped state is much smaller than the recoil energy, which is the limit we would avoid in this letter.

In fact, for our interest, the precise shape of the potential is of little importance, as long as the ground state wavefunction at each site is *sufficiently elongated* and pointing towards the center of each hexagon. We call this elongated wavefunction an “orbital dimer”, because its spatial symmetry mimics that of a link variable defined on bonds. To make this analogy precise, we perform a site-to-bond duality transformation. As shown in Fig. 1(a), under this mapping, an atom/molecule localized at a site of the original Kagome lattice (solid lines) becomes a dimer residing on a bond of the dual triangular lattice (dashed lines). Accordingly, particles on the original lattice are mapped to dimers on the dual lattice [23].

Dipolar interactions. If the dipolar particles are polarized in the z -direction by an external field, their interaction is given by the long-range potential $V_{dd}(\mathbf{r}) = d^2(1 - 3z^2/r^2)/r^3$. Here, d is the dipole moment, r is the distance between the two dipoles, and z is the z -

component of \mathbf{r} . For a quasi-2D system, the dipolar interaction is repulsive near the xy -plane, which leads to energy penalties for particles close to each other. The largest interaction is the on-site repulsion U and the next one is the repulsion between particles on the same hexagon of the original lattice, or equivalently dimers joining at the same site on the dual lattice. Three such configurations $i = 1, 2, 3$ are shown in Fig. 2(a)-(c). Even smaller is the interaction for parallel (V_{\parallel}) and staggered (V_S) dimers, shown in Figs. 2(d) and 2(e), respectively. The effect of longer-range interactions will be studied below. In the limit $U > V_i \gg V_{\parallel} > V_S$, below a critical filling ($1/6$ for the Kagome lattice), the large energy cost V_i ($i = 1, 2, 3$) forbids dimers to share a common site on the dual lattice. This enforces the “hard-core constraint”, a key feature of QDMs. At the critical filling, the dual lattice is “fully covered” by dimers. Namely, among the six bonds connected to any site, one and only one bond is occupied by a dimer.

We now show that the desired hierarchy of interactions given above can be satisfied by controlling the dipolar interactions and increasing the elongation of Wannier wavefunctions. For this purpose, we approximate the Wannier function at each site of the Kagome lattice by these Gaussian “atomic orbitals”,

$$w(x, y, z) = (\alpha\beta\gamma)^{-1/2}\pi^{-3/4} \exp\left[-\frac{x^2}{2\alpha^2} - \frac{y^2}{2\beta^2} - \frac{z^2}{2\gamma^2}\right],$$

with $\alpha > \beta \gg \gamma$. Here, a strong laser field in the z direction is used to confine the particles within the xy plane (γ being small) and the x axis is chosen to be along the direction of the double-well potential as shown in Fig. 1(c). This simple ansatz would not provide an accurate value for U and V_S , but it suffices to estimate their order of magnitude and demonstrate the proper limit in which our system could be mapped to a QDM.

Within this ansatz, we find

$$U \simeq d^2 \sqrt{\frac{2}{\pi}} \left[\frac{2}{3\alpha\beta\gamma} - \frac{E(1 - \alpha^2/\beta^2)}{\alpha^2\beta} \right].$$

where $E(x)$ is the complete elliptic integral of the second kind. For tight confinement (small β and γ), U is exceedingly large, so it disfavors multi-occupancy of the same lattice site. On the dual lattice, this means that there can be at most one dimer on each bond. It is also straightforward to compute the corresponding interaction V_i . For example,

$$V_3 = \frac{d^2}{r^3} \sqrt{\frac{2}{\pi}} \int_0^{\frac{\pi}{2}} d\theta \sec^3 \theta e^{-\frac{y}{2}} (y^{\frac{5}{2}} - y^{\frac{3}{2}}) + \frac{d^2 \sqrt{8\pi}}{3\alpha\beta\gamma} e^{-\frac{r^2}{2\alpha^2}},$$

where $y(\theta) = r^2/(\alpha^2 + \beta^2 \tan^2 \theta)$, and r is the distance between the center of two dimers.

Since the lattice structure is unspecified and can vary arbitrarily [21], we can treat α , β , and γ as free controlling parameters and show that the limit $U > V_i \gg V_{\parallel} >$

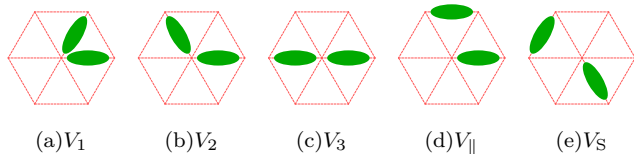


FIG. 2: (Color online) Interactions between dipolar particles on the dual triangular lattice shown in Fig. 1.

V_S can be achieved with elongated Wannier functions. First, it is useful to consider the case of isotropic Wannier functions, $\alpha = \beta$, and small wavefunction overlap, $\alpha \ll r$ with r being the distance between two lattice sites. Then, the interaction energy is reduced to d^2/r^3 , and the ratio $V_1 : V_2 : V_3 : V_{\parallel} : V_S$ is $8 : 1.54 : 1 : 1 : 0.43$. In particular, we see that V_2 and V_{\parallel} are of the same order. A key point of our proposal is that by using elongated Wannier functions, the dipolar interaction for configuration $i = 2, 3$ can be boosted with respect to the parallel configuration, since they have much larger wave function overlap (schematically shown in Fig. 2). For example, for $\alpha = 0.3$ and $\beta = 0.1$ (in the units of the lattice constant), the ratio $V_1 : V_2 : V_3 : V_{\parallel} : V_S$ becomes $30 : 8.6 : 8.6 : 1 : 0.49$ for $\gamma = \beta/10$ and $21 : 5.8 : 5.6 : 1 : 0.49$ for $\gamma = \beta/5$. Here V_3 is almost one order of magnitude larger than V_{\parallel} and their ratio can be further enhanced by increasing the elongation of the Wannier function (through adjusting the optical lattice) and/or reducing γ . Notice that γ can be tuned independently. For a lattice with sufficient elongated Wannier functions, the mapping to QDM becomes asymptotically accurate as γ is reduced.

The orbital dimer model. At the critical filling, the low-energy fluctuations of the system are described by the following Hamiltonian after projecting out high-energy degrees of freedom (at the scale of U and V_i),

$$H = -t_{\text{eff}} \sum \left(|\nabla\rangle\langle\nabla| + h.c. \right) + V_{\text{eff}} \sum \left(|\nabla\rangle\langle\nabla| + |\nabla\rangle\langle\nabla| \right) + V_{LR}, \quad (2)$$

where the summation is over all flippable plaquettes [5] and V_{LR} describes higher order terms due to longer-range interactions (beyond those shown in Fig. 2). Here the dimer has the same statistical property as the constituent particle, so it could be either *bosonic* or *fermionic*. At the critical filling, the dual triangular lattice is fully covered by the orbital dimers. All local density fluctuations are gapped out due to large energy penalty of V_i ($i = 1, 2, 3$). Hence density remains homogeneous on large length scales and the dominant effect of longer-range repulsive interaction is to contribute a constant shift in the free energy. As a leading order approximation, we will drop V_{LR} in the low-energy effective Hamiltonian Eq. (2) and expect the orbital dimer model captures the essential low-energy physics of the system.

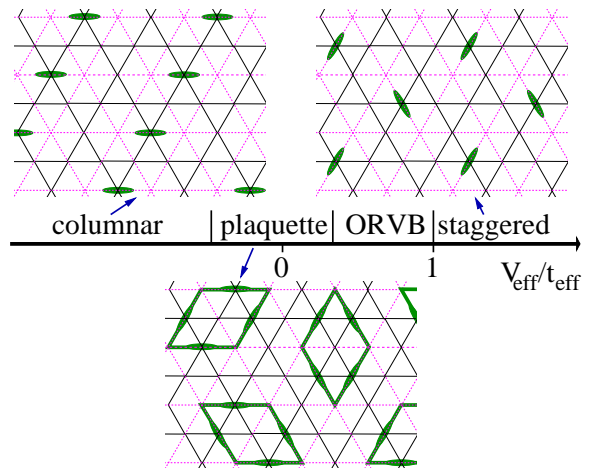


FIG. 3: (Color online) The phase diagram for the bosonic particles and the particle configuration in the crystalline phases.

At the critical filling, particle hopping gives rise to overlapping dimers (sharing the same site), which costs energy of order V_i . Such virtual hopping processes lead to quantum resonance of orbital dimers around a plaquette (t_{eff}), as well as corrections to V_{\parallel} and V_S through second order perturbations, of order t^2/V_i . To the leading approximation, we use one (average) energy scale t to estimate the amplitudes of relevant hoppings. The repulsive interaction between two parallel dimers, V_{eff} , is set by the energy scale $V_{\parallel} - V_S$ up to corrections of $O(t^2/V_i)$. By varying t and the interacting strength, t_{eff} and V_{eff} can be tuned to explore various parameter ranges of the QDM, except for the limit of $V_{\text{eff}} \ll -t^2/V_i$, since $V_{\parallel} > V_S$ for dipolar interaction. To estimate the relevant energy scales, we take $d = 0.1$ Debye, $a = 0.25\mu\text{m}$, $V_1 \sim 4V_{2,3} \sim 20V_{\parallel}$, and $t \sim 10\text{nK}$. Then, $V_{\text{eff}} \sim V_{\parallel} - V_S \sim 2.3\text{nK}$ and $t_{\text{eff}} \sim 2t^2/V_1 \sim 2.16\text{nK}$. This shows that the condition $U, V_i \gg V_{\text{eff}} \sim t_{\text{eff}} \gg T$ can be satisfied.

For bosonic particles, the phase diagram at the critical filling is shown in Fig. 3, using the knowledge of QDM [5]. As $V_{\text{eff}}/t_{\text{eff}}$ increases, four phases appear consequently: the columnar phase, the $\sqrt{12} \times \sqrt{12}$ plaquette phase ($V_{\text{eff}}/t_{\text{eff}} \sim 0$), the ORVB topological phase ($V_{\text{eff}}/t_{\text{eff}} \lesssim 1$), and the staggered phase ($V_{\text{eff}}/t_{\text{eff}} > 1$). In the staggered and the columnar phases, the dimers are frozen in the ground state, while in the $\sqrt{12} \times \sqrt{12}$ state, they can resonate in each plaquette marked by the thick lines in Fig. 3. In terms of dipolar particles, all these three phases correspond to various commensurate charge-density-wave states, which break the point group symmetry of the underlying lattice. On the other hand, all the spatial symmetries of the lattice are preserved in the ORVB phase. However, this state has critical dependence on the topology of the underlying manifold. On a topologically nontrivial manifold, it shows degenerate ground states, topologically distinct from one another,

known as topological degeneracy. As a Z_2 topological phase, the ORVB phase has 4 degenerate ground states distinguished by two Z_2 topological indices if placed on a torus. As discussed below, the phenomenon of topological degeneracy not only provides unique experimental signatures for the ORVB phase, but also leads to the possibility of realizing quantum memory.

In the context of frustrated spins the RVB state has two different types of fractional excitations: spinons (carrying spin $1/2$) and holons (carrying charge e), known as the spin-charge separation. For an ORVB state, however, the orbital dimers are not spin singlets, and hence spinon excitations are forbidden. As a result, only one type of fractional excitations, holons, emerges. A holon carries only half the quantum number of an underlying dipolar particle, e.g., a half dipole, while the statistics of a holon may depend on microscopic details of the system [26]. This phenomenon shares strong similarities with the deconfined monopole excitations in spin ice [27].

Using different optical lattices of double-well potentials, QDM on other lattices can also be achieved through similar constructions. For example, the following laser intensity results in a square-lattice QDM,

$$I = I_1 \sum_{i=1,2} \cos^2(\mathbf{k}_i \cdot \mathbf{r}) + I_2 \sum_{j=1,2} \cos^2(\mathbf{q}_j \cdot \mathbf{r}). \quad (3)$$

with the in-plane component satisfying $|\mathbf{q}_j| = 3|\mathbf{k}_i|/\sqrt{2}$ and the azimuth angles: $\theta_{\mathbf{k}_i} = (2i+1)\pi/4$ and $\theta_{\mathbf{q}_j} = 2j\pi/4$. In this case, the ORVB phase shrinks into a RK point as expected for all bipartite lattices, while the crystalline phases remain to occur in regions with dimer configurations slightly different from the triangular lattice.

Experimental detection. Each of the phases discussed above displays a distinct interference pattern in Bragg scattering experiments. In the lattice shown in Fig. 1, for example, the ORVB phase has Bragg peaks at wavevectors commensurate with the reciprocal vectors of the lattice: $(2\pi, 2\pi/\sqrt{3})$ and $(0, 4\pi/\sqrt{3})$. In the staggered phase, however, the Bragg peaks are located at $(m\pi, 2n\pi/\sqrt{3})$ for any integer m and n . Similarly, the columnar phase [Bragg peaks commensurate with vectors $(\pi, \sqrt{3}\pi)$ and $(0, 4\pi/\sqrt{3})$] and the $\sqrt{12} \times \sqrt{12}$ phase [with vectors $(\pi/3, \pm\pi/\sqrt{3})$] can also be distinguished. The six-fold rotational symmetry is broken in the staggered and columnar phase. This can be used to distinguish them from other phases in time-of-flight experiments.

As in the experimental search for spin liquids, lack of symmetry breaking at low temperatures is an evidence of the ORVB phase in our system. One way to distinguish it from the topologically trivial state is to detect the topological degeneracy in, for example, the “annulus” geometry, which can be achieved by punching a hole on the 2D optical lattice using an extra laser beam to form a forbidden region with high energy barrier. For a large enough hole, the ORVB ground state is doubly degenerate. The two topologically-distinct degenerate states

can serve as a “qubit” [28]. It can be “flipped” by creating a pair of holons and then annihilating them after moving one holon around the hole of the annulus. Furthermore, topological quantum memory can be realized by punching multiple holes and manipulating the holons. For a hole of finite size, tunneling lifts the degeneracy and results in two nearly-degenerate states. The energy splitting increases upon reducing the size of the hole. The size dependence of the energy splitting can serve as a direct evidence of Z_2 topological order. However, it is challenging to measure the splitting, which is on the order of pK , experimentally. Another distinct feature of the ORVB state is the holons. How to efficiently probe such fractional excitations remains an important open problem.

We thank Sankar Das Sarma, Eduardo Fradkin, Han Pu, Hong Yao, and especially Christopher Henley for helpful discussions. This work is supported by the Office of Science, U.S. Department of Energy under Contracts DE-FG02-91ER45439 of the Frederick Seitz Materials Research Laboratory at the University of Illinois, JQI-NSF-PFC and JQI-AFOSR-MURI at Maryland (KS), U.S. Army Research Office Grant No. W911NF-07-1-0293 (EZ and WV), NIST Grant 70NANB7H6138 Am 001 and ONR Grant N00014-09-1-1025A (EZ), and the CAS/SAFEA International Partnership Program for Creative Research Teams of China (WV).

-
- [1] X. G. Wen, Phys. Rev. B **44**, 2664 (1991).
 - [2] C. Nayak *et al.*, Rev. Mod. Phys. **80**, 1083 (2008).
 - [3] S. A. Kivelson, D. S. Rokhsar, and J. P. Sethna, Phys. Rev. B **35**, 8865 (1987).
 - [4] D. S. Rokhsar and S. A. Kivelson, Phys. Rev. Lett. **61**, 2376 (1988).
 - [5] R. Moessner and S. L. Sondhi, Phys. Rev. Lett. **86**, 1881 (2001).
 - [6] N. Read and S. Sachdev, Phys. Rev. Lett. **66**, 1773 (1991).
 - [7] C. Mudry and E. Fradkin, Phys. Rev. B **49**, 5200 (1994).
 - [8] A. Kitaev, Ann. Phys. (NY) **303**, 2 (2003).
 - [9] T. Senthil and M. P. A. Fisher, Phys. Rev. B **62**, 7850 (2000).
 - [10] R. Moessner, S. L. Sondhi, and E. Fradkin, Phys. Rev. B **65**, 024504 (2001).
 - [11] N. R. Cooper, Adv. Phys. **57**, 539 (2008).
 - [12] A. F. Albuquerque, H. G. Katzgraber, M. Troyer, and G. Blatter, Phys. Rev. B **78**, 014503 (2008).
 - [13] R. Moessner, S. L. Sondhi, and P. Chandra, Phys. Rev. Lett. **84**, 4457 (2000).
 - [14] R. Moessner and S. L. Sondhi, Phys. Rev. B **63**, 224401 (2001).
 - [15] L. Balents, M. P. A. Fisher, and S. M. Girvin, Phys. Rev. B **65**, 224412 (2002).
 - [16] S. V. Isakov, Y. B. Kim, and A. Paramekanti, Phys. Rev. Lett. **97**, 207204 (2006).
 - [17] K.-K. Ni *et al.*, Science **322**, 231 (2008).
 - [18] S. Ospelkaus *et al.*, arXiv:0811.4618v1 (unpublished).
 - [19] T. Lahaye *et al.*, Rep. Prog. Phys. **72**, 126401 (2009).

- [20] In this letter, a duality relation is always referred to as this site-to-bond mapping.
- [21] W. S. Bakr *et al*, arXiv:0908.0174v1 (unpublished).
- [22] L. Santos *et al*, Phys. Rev. Lett. **93**, 030601 (2004).
- [23] Related mappings in toy models of electronic systems without elongating the wavefunction were studied in Refs. 24, 25.
- [24] M. Freedman, C. Nayak, and K. Shtengel, Phys. Rev. Lett. **94**, 066401 (2005).
- [25] H. Yao, (private communication).
- [26] S. Kivelson, Phys. Rev. B **39**, 259 (1989).
- [27] C. Castelnovo, R. Moessner, and S. L. Sondhi, Nature **451**, 42 (2008).
- [28] R. Moessner and S. L. Sondhi, Prog. Theor. Phys. Suppl. **145**, 37 (2002).